Electronic Supplementary Material (ESI) for RSC Advances.
This journal is © The Royal Society of Chemistry 2023

Supporting Information

Component-Controlled Synthesis of Pd_xSn_y Nanocrystals on Carbon Nanotubes as Advanced Electrocatalysts for Oxygen Reduction Reaction

Weibin Guo,[a] Rui Yang,[bc] Jiayao Fan,[b] Xing Xiang,[a] Xuehui Du,[a] Naien Shi,*[ac] Jianchun Bao,[b] and Min Han*[ab]

[a] Fujian Cross Strait Institute of Flexible Electronics (Future Technologies), Fujian Normal University, Fuzhou 350117, P. R. China

[b] Jiangsu Key Laboratory of New Power Batteries, and Jiangsu Key Laboratory of Biofunctional Materials, School of Chemistry and Materials Science, Nanjing Normal University, Nanjing 210023, P. R. China

[c] Key Laboratory for Organic Electronics and Information Displays, Institute of Advanced Materials, Nanjing University of Posts & Telecommunications, Nanjing 210023, P. R. China

E-mail: ifeneshi@fjnu.edu.cn (N. Shi); 07203@njnu.edu.cn (M. Han)

Additional Experimental Sections

1. Koutecky-Levich (K-L) plots.

The related ORR polarization curves of Pd_3Sn/CNTs NHs at the rotating rate of 400, 800, 1200, 1600, and 2500 rpm were obtained. Based on those polarization curves, the electron transfer number (*n*) per oxygen molecule involved in the ORR process was calculated according to the Koutecky-Levich (K-L) equation as follows:

$$\frac{1}{J} = \frac{1}{J_K} + \frac{1}{B\omega^{0.5}} \quad (1)$$

Where J is the current density, J_k is the kinetic current density, ω is the rotating rate of the electrode, and B could be obtained from the K-L plots using the equation (1). The electron transfer number (n) per oxygen molecule involved in the ORR process could be calculated from the slope (B) of the linear plot and the following relationship:

$$B = 0.62nF(D_{O_2})^{2/3}v^{-1/6}C_{O_2} \quad (2)$$

F in equation (2) is the Faraday constant (96485 C mol^{-1}), D_{O2} is the diffusion coefficient of O_2 in 0.1 M KOH (1.9×10^{-5} cm^2 s^{-1}), v is the kinetic viscosity (0.01 cm^2 s^{-1}), C_{O2} is the bulk concentration of O_2 (1.2×10^{-6} mol cm^{-3}), and the value of *n* represents the number of transferred electrons in the ORR process.

2. Rotating ring-disk electrode (RRDE) measurements.

The rotating speed of the working electrode was fixed at 1600 rpm with the scan rate of 5 mV s^{-1} in O_2-saturated 0.1 M KOH solution for the RRDE test. The HO_2^- % and the electron transfer number (*n*) involved in the ORR process were determined by the following equations:

$$HO_2^-\% = 200(I_r/N)/(I_d + I_r/N) \quad (3)$$

$$n = 4I_d/(I_d + I_r/N) \quad (4)$$

Where I_d is the disk current, I_r is the ring current, and N is the current collection efficiency of the Pt ring, which is identified to be 0.43 in 2 mmol L^{-1} $K_3[Fe(CN)_6]$ and 0.1 mol L^{-1} KCl solution.

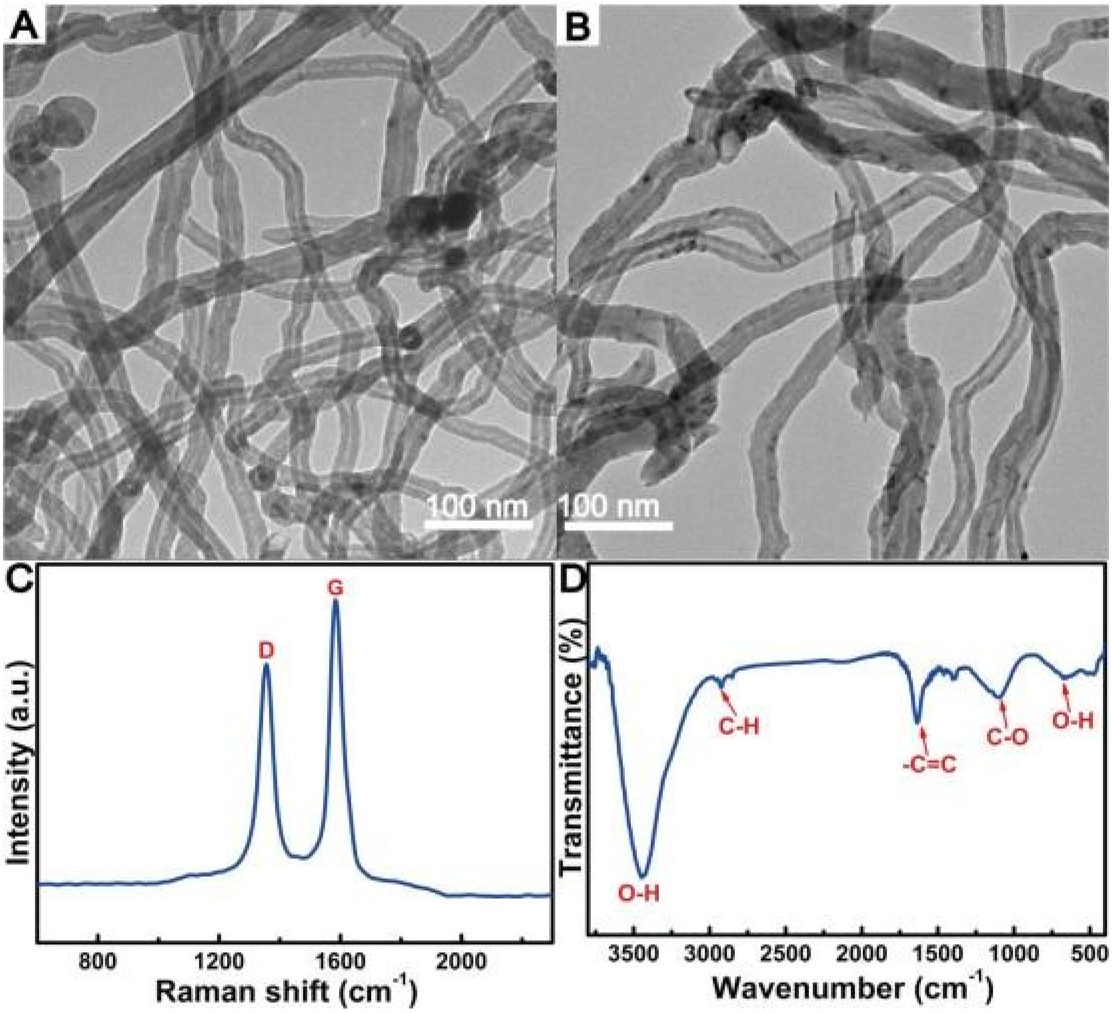

Fig. S1 A-B) TEM images of the carbon nanotubes (CNTs) before (A) and after (B) acidic treatment. C-D) Raman (C) and FT-IR (D) spectra of the CNTs after acidic treatment.

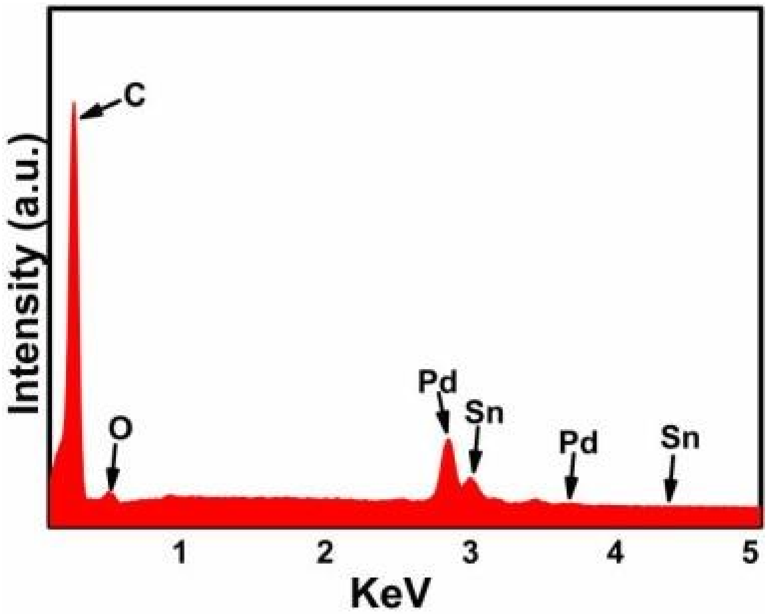

Fig. S2 The EDS pattern for the typical Pd_3Sn/CNTs NHs.

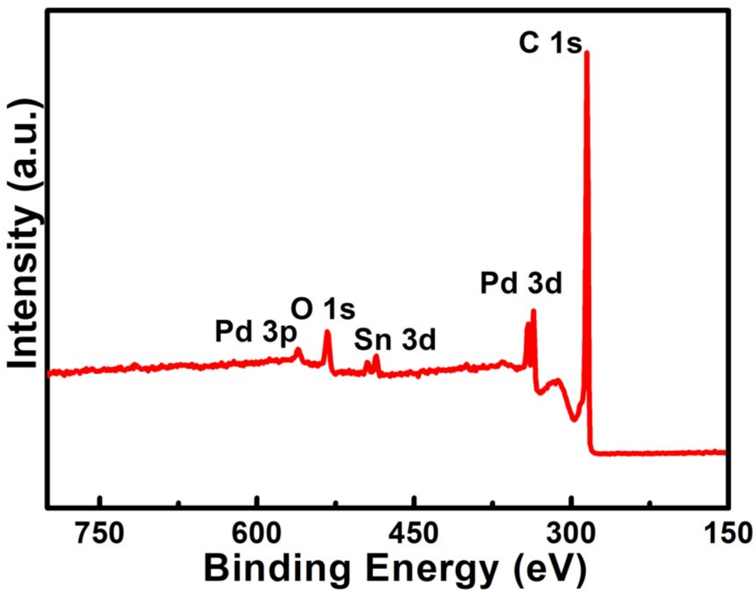

Fig. S3 The survey XPS spectra for the typical Pd_3Sn/CNTs NHs.

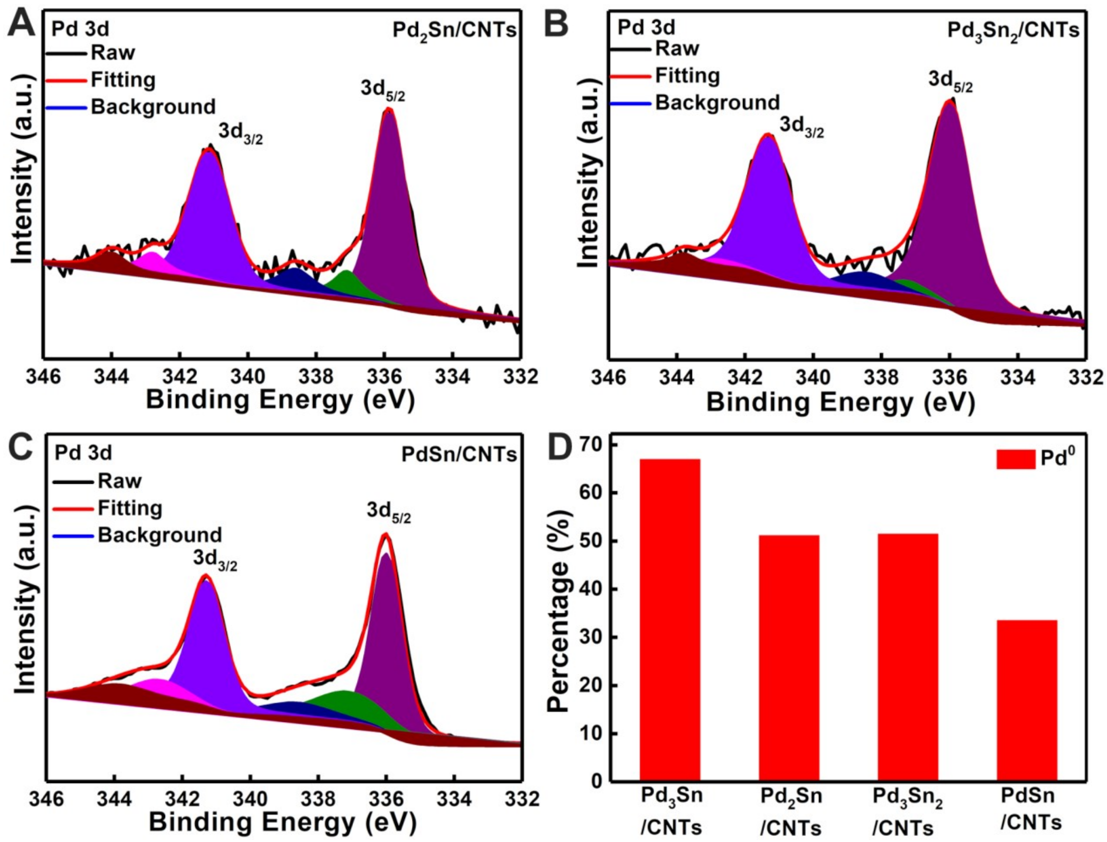

Fig. S4 A-C) Pd 3d fine XPS spectra for the Pd_2Sn/CNTs NHs (A), Pd_3Sn_2/CNTs NHs (B) and PdSn/CNTs NHs (C). D) The percentage of Pd^0 for the Pd_3Sn/CNTs NHs, Pd_2Sn/CNTs NHs, Pd_3Sn_2/CNTs NHs, and PdSn/CNT NHs.

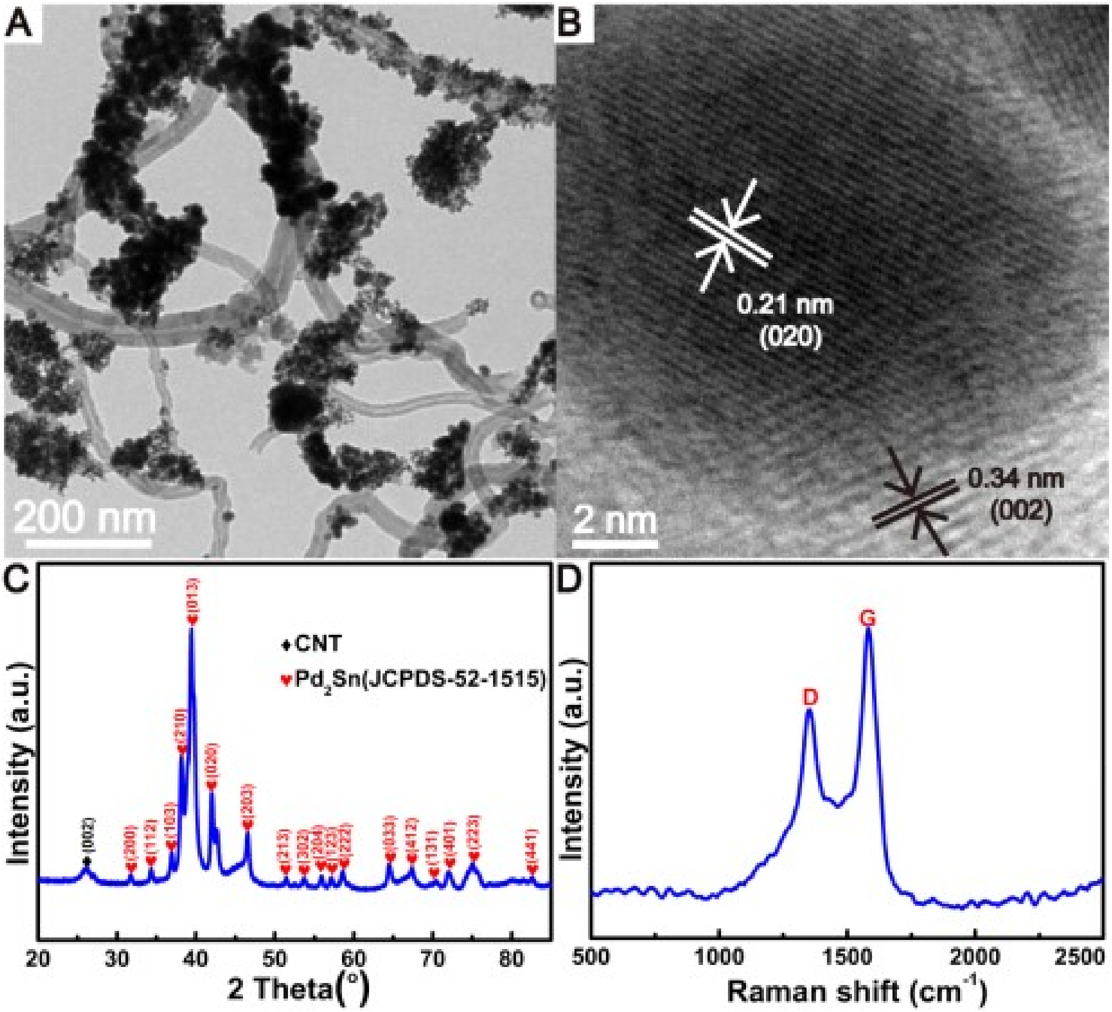

Fig. S5 A-B) TEM image (A) and HRTEM image (B) of Pd_2Sn/CNTs NHs. C-D) The corresponding XRD pattern (C) and Raman spectra (D) for Pd_2Sn/CNTs NHs.

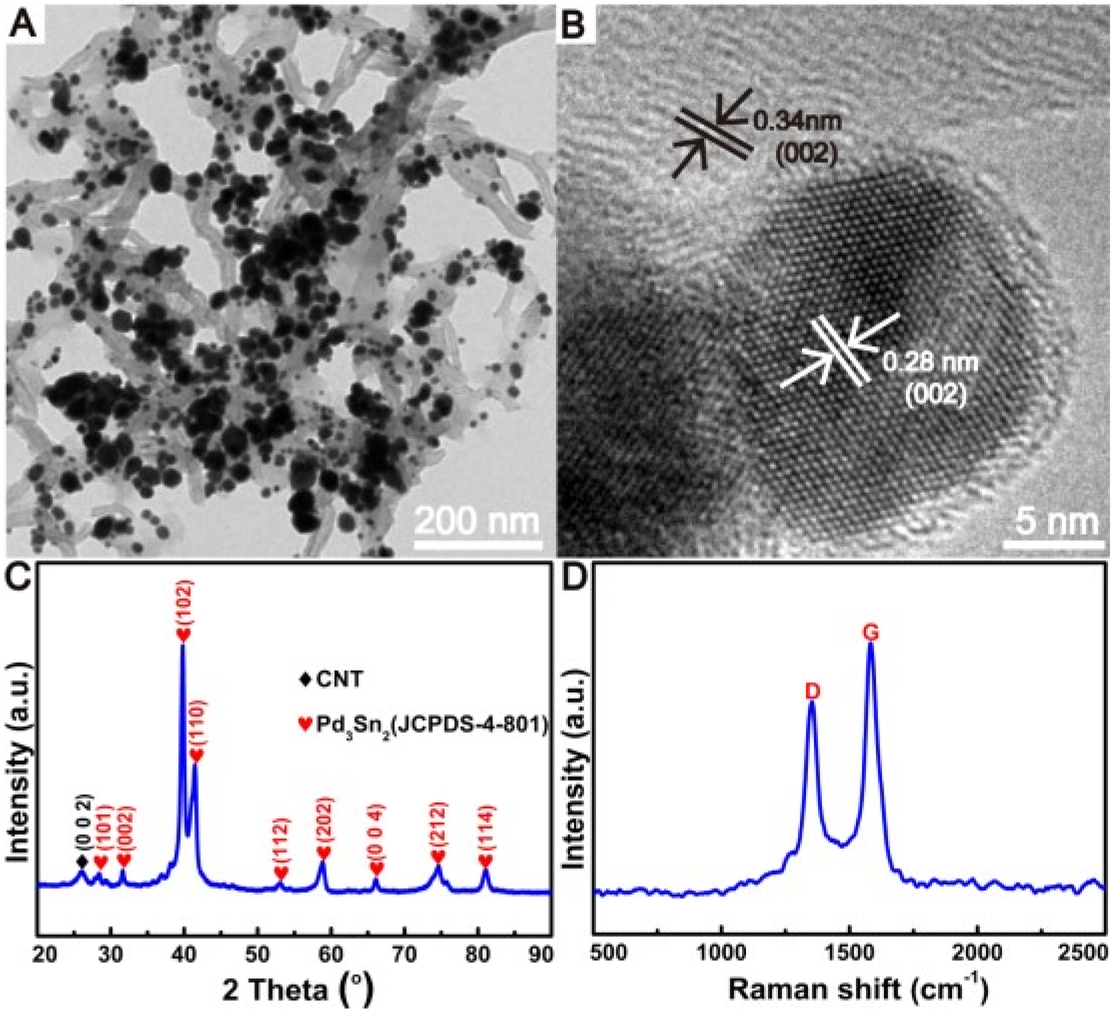

Fig. S6 A-B) TEM image (A) and HRTEM image (B) of Pd_3Sn_2/CNTs NHs. C-D) The related XRD pattern (C) and Raman spectra (D) for Pd_3Sn_2/CNTs NHs.

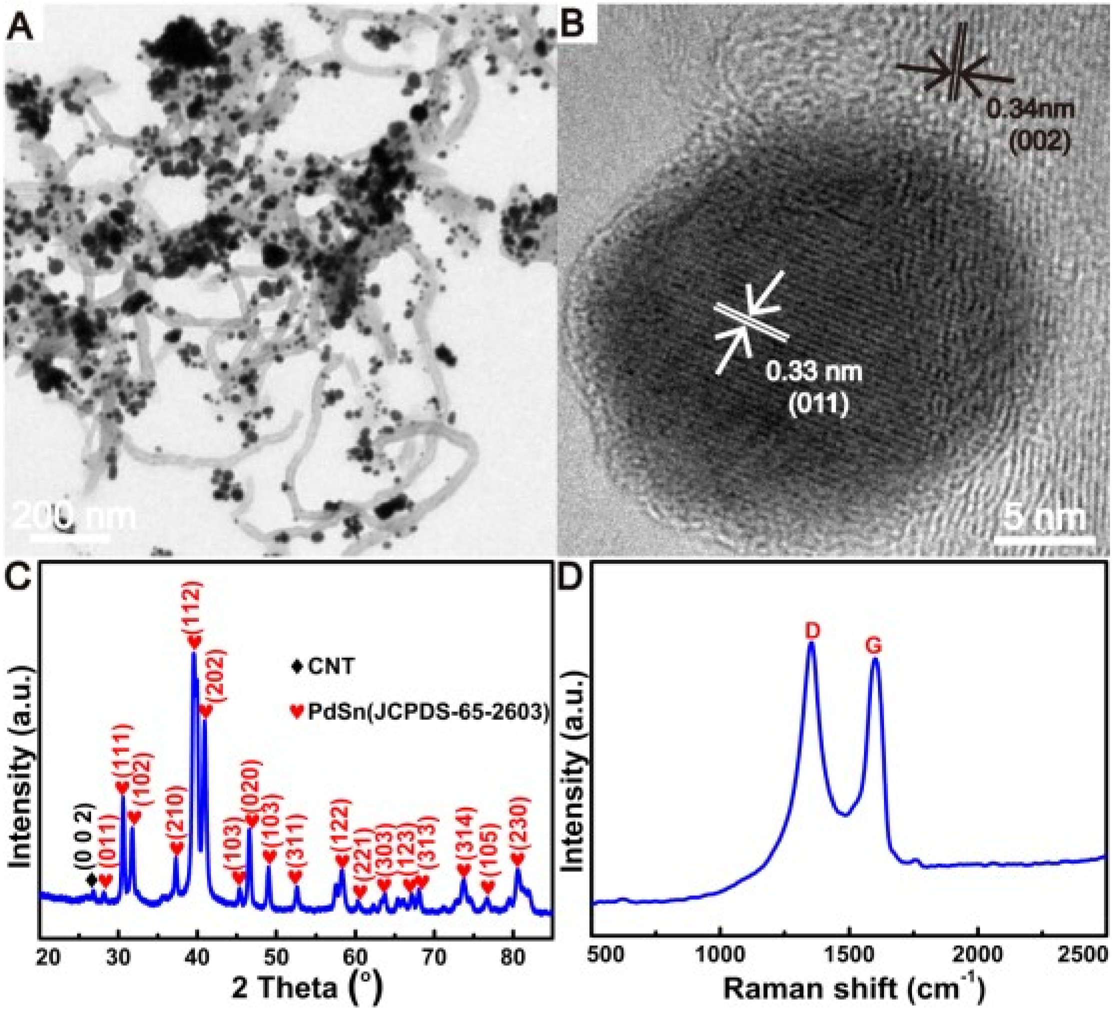

Fig. S7 A-B) TEM image (A) and HRTEM image (B) of PdSn/CNTs NHs. C-D) The related XRD pattern (C) and Raman spectra (D) for PdSn/CNTs NHs.

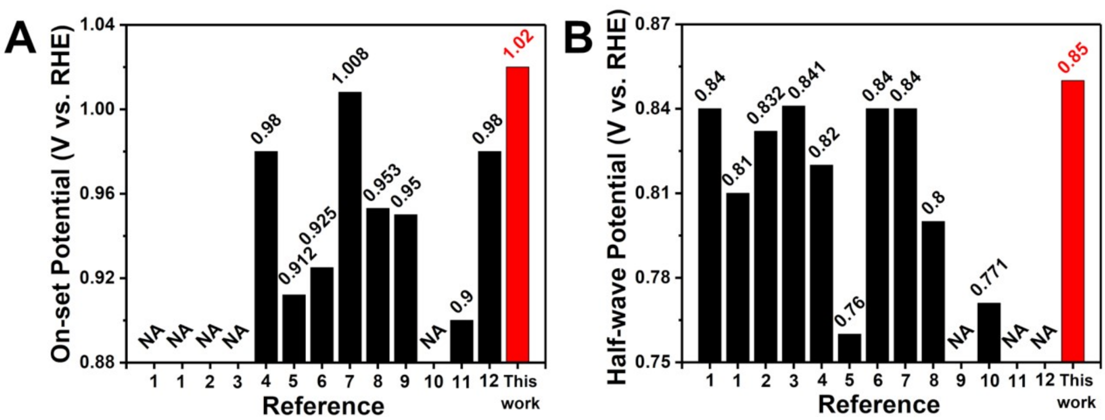

Fig. S8 A-B) The on-set potential (A) and half-wave potential (B) of Pd_3Sn/CNTs NHs and recently reported Pd-based alloys and multimetallic catalysts [1-12].

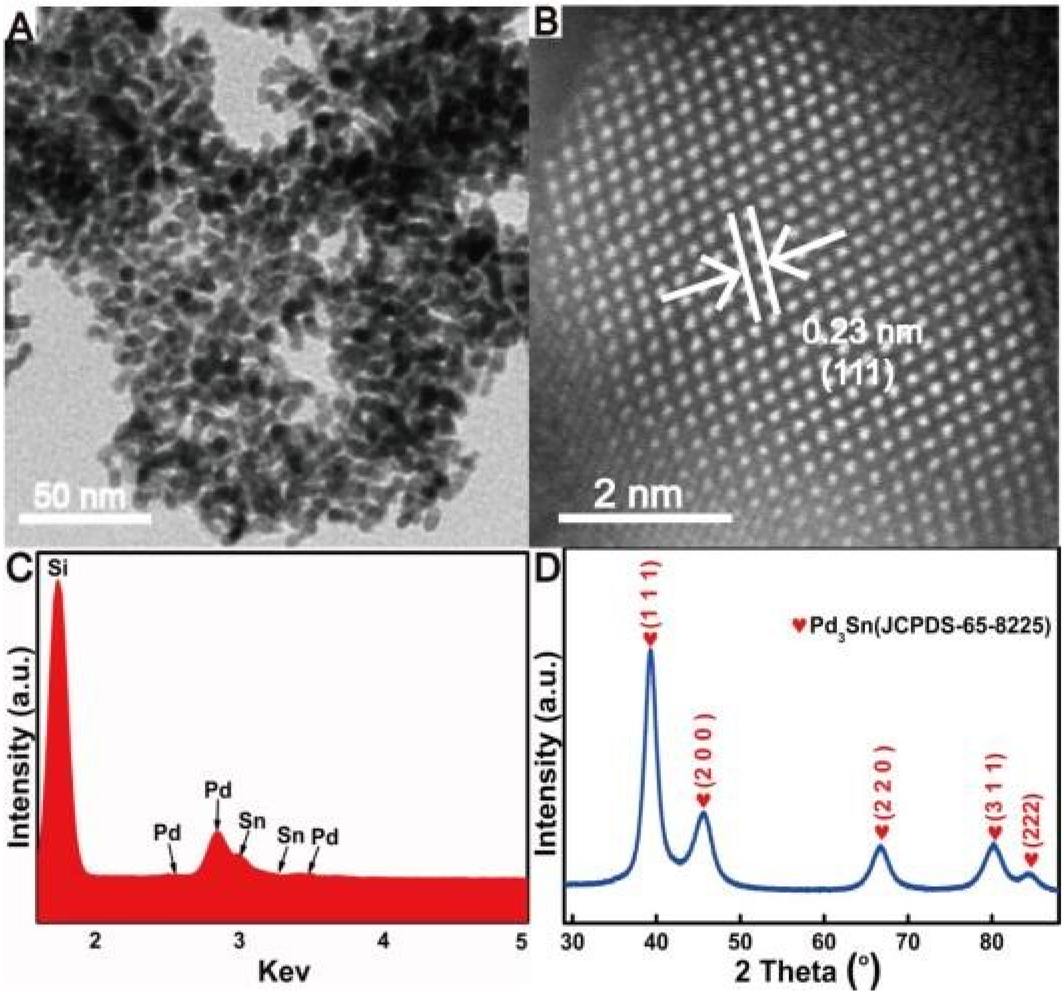

Fig. S9 A-B) TEM image (A) and HRTEM image (B) of pure Pd_3Sn NCs. C-D) The corresponding EDS spectra (C) and XRD pattern (D) for pure Pd_3Sn NCs.

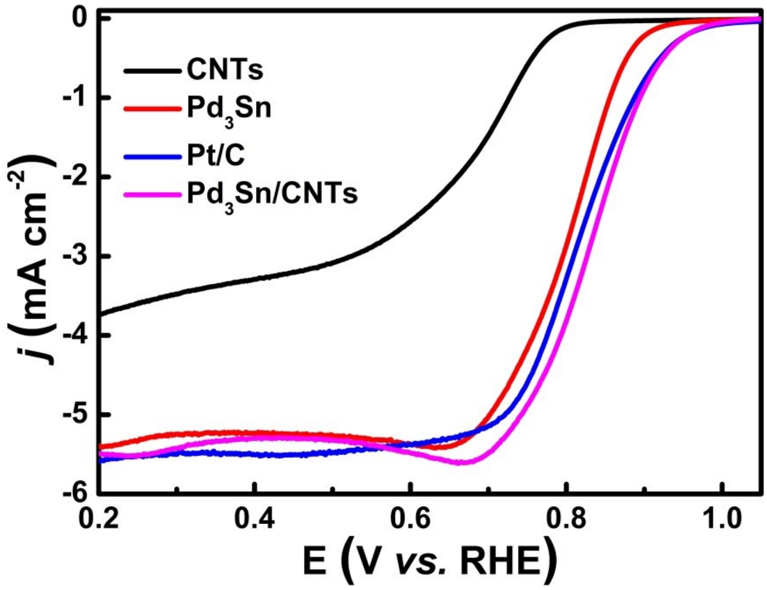

Fig. S10 ORR polarization plots of pure CNTs, pure Pd_3Sn NCs, commercial Pt/C, and Pd_3Sn/CNTs NHs in O_2-saturated 0.1 M KOH electrolyte at the electrode rotation rate of 1600 rpm.

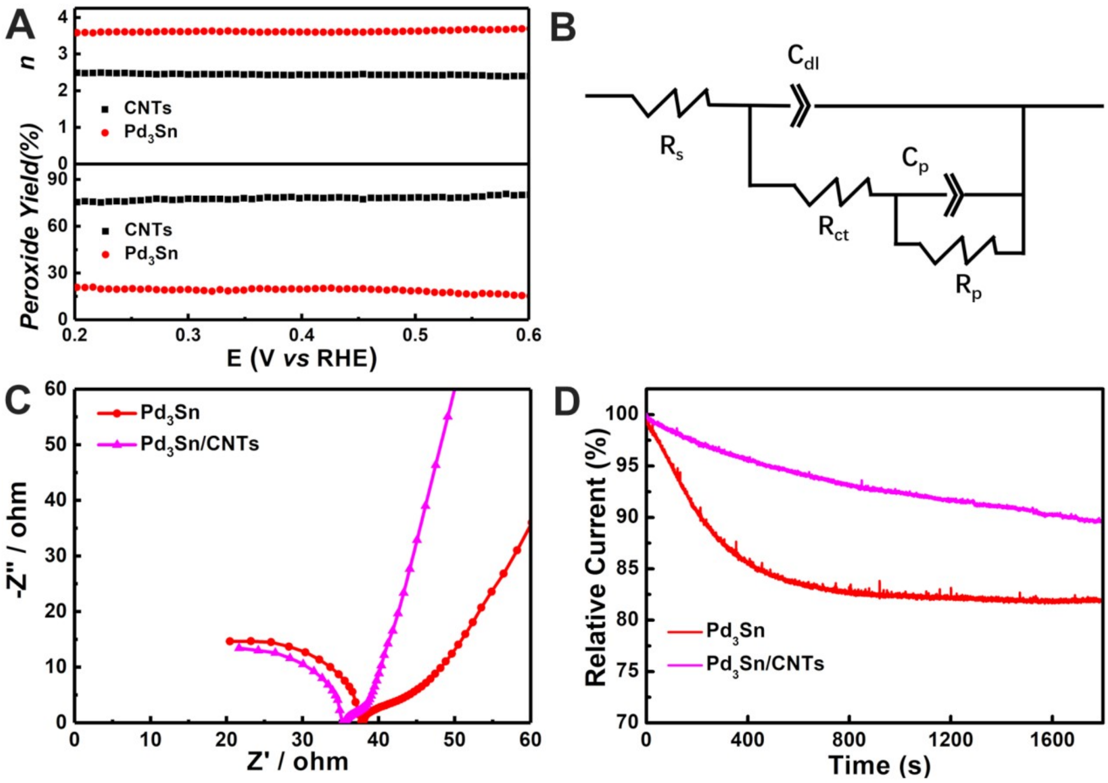

Fig. S11 A) The peroxide species yield and the number of transferred electrons (*n*) for pure CNTs and pure Pd_3Sn NCs. B) The equivalent circuit model. C-D) Nyquist plots

(C) and i-t plots (D) for pure Pd_3Sn NCs and Pd_3Sn/CNTs NHs.

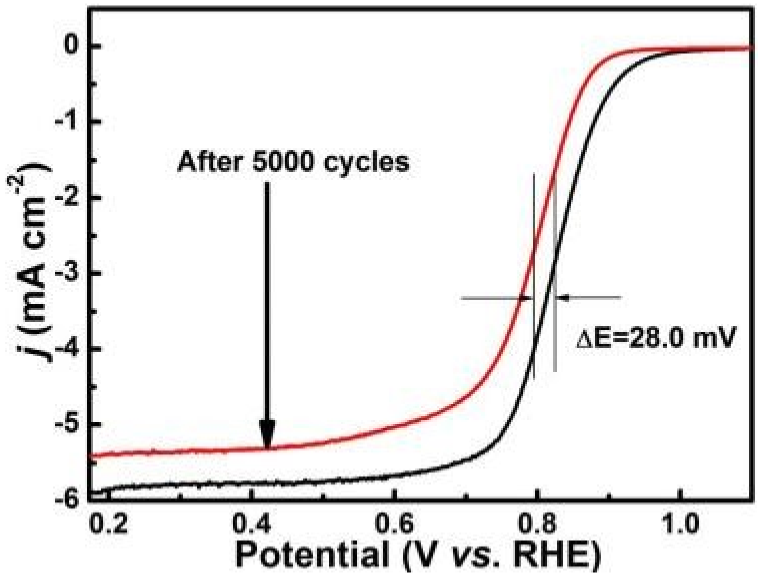

Fig. S12 The durability test plots for the commercial Pt/C catalyst.

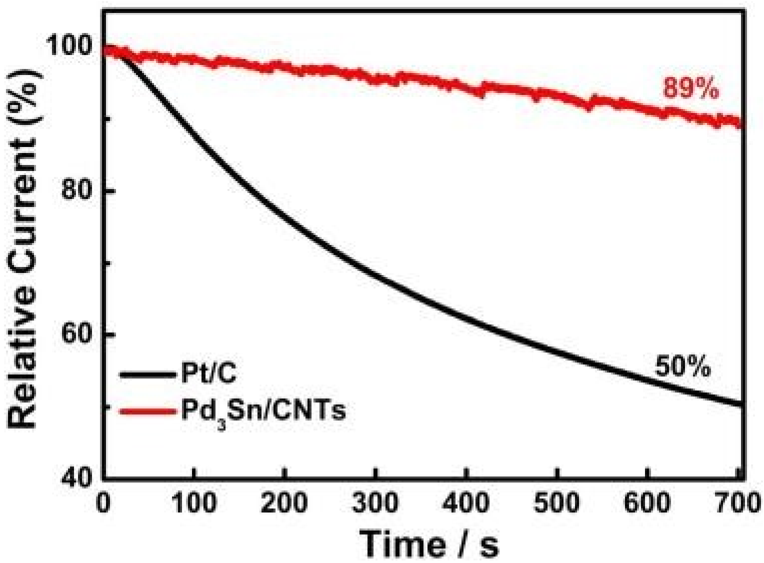

Fig. S13 Durability evaluation of the typical Pd_3Sn/CNTs NHs and Pt/C catalyst in O_2-saturated 0.1 M KOH + 1 M CH_3OH solution at a constant potential of 0.7 V (*vs.* RHE) for 700s with the electrode rotation rate of 1600 rpm.

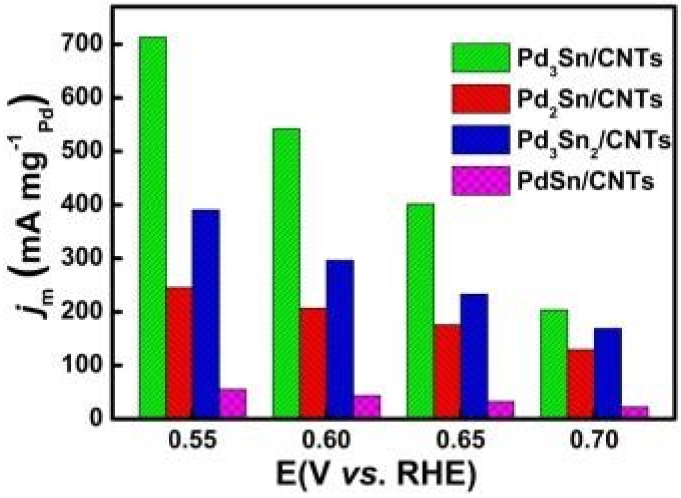

Fig. S14 Mass-specific activities of Pd_xSn_y/CNTs NHs catalysts at the potential of 0.55, 0.60, 0.65, and 0.70V (*vs*. RHE) according to the mass of pure Pd in the NHs.

Table S1. Comparison of catalytic performance parameters of Pd_3Sn/CNTs NHs in this work with recently reported Pd-based alloys and multimetallic catalysts.

Pd-based nanocatalysts	Electrolyte	On-set Potential (V *vs.* RHE)	Half-wave Potential (V vs. RHE)	References
PbPd/C_Pre[1]	0.1 M KOH	NA	0.84	*J. Electroanal. Chem.* **2022**, *917*, 116391.
SnPd/C_300[1]	0.1 M KOH	NA	0.81	
Pd/SnO_2[2]	0.1 M KOH	NA	0.832	*J. Colloid Interface Sci.* **2021**, *602*, 159-167.
Pd/Nb_2O_5[3]	0.1 M KOH	NA	0.841	*Dalton Trans.* **2020**, *49*, 1398-1402.
Pd@Zn_Core-shell[4]	0.1 M KOH	0.98	0.82	*J. Catal.* **2020**, *382*, 181-191.
N-rGO-Pd[5]	0.1 M KOH	0.912	0.76	*Int. J. Hydrogen Energy* **2018**, *43*, 5690-5702.
Pd nanonetworks[6]	0.1 M KOH	0.925	0.84	*Int. J. Hydrogen Energy* **2018**, *43*, 229-238.
$Ir_{27}Pd_{73}/C$[7]	0.1 M NaOH	1.008	0.84	*J. Electroanal. Chem.* **2018**, *827*,120-127.
$MnPd_3/C$[8]	0.1 M KOH	0.953	0.80	*ACS Appl. Mater Interfaces* **2018**, *10*, 8155-8164.
Pd_2CoAg[9]	0.1 M KOH	0.95	NA	*Appl. Catal., B* **2018**, *241*, 424-429.
PdAuCu[10]	0.1 M KOH	NA	0.771	*ChemSusChem* **2017**,

				10, 1469-1474
Pd-g-C_3N_4[11]	0.1 M KOH	0.90	NA	*J. Phys. Chem. C* **2016**, *120*, 14467 -14473.
Pd_3Pb/TiO_2[12]	0.1 M KOH	0.98	NA	*J. Appl. Electrochem.* **2016**, *46*, 745-753.
Pd_3Sn/CNTs NHs	**0.1 M KOH**	**1.02**	**0.85**	**This work**

References:

1 M. Lüsi, H. Erikson, H.-M. Piirsoo, P. Paiste, J. Aruväli, A. Kikas, V. Kisand, A. Tamm, K. Tammeveski, J. Electroanal. Chem., 2022, 917, 116391.

2 G. Chao, L. Zhang, T. Xue, J. Tian, W. Fan, T. Liu, J. Colloid Interface Sci., 2021, 602, 159-167.

3 C. Huang, W. Dong, C. Dong, X. Wang, B. Jia, F. Huang, Dalton Trans., 2020, 49, 1398-1402.

4 H. Yang, K. Wang, Z. Tang, Z. Liu, S. Chen, J. Catal., 2020, 382, 181-191.

5 A. Ejaz, S. Jeon, Int. J. Hydrogen Energy, 2018, 43, 5690-5702.

6 H. Begum, M. S. Ahmed, S. Cho, S. Jeon, Int. J. Hydrogen Energy, 2018, 43, 229-238.

7 A. T. N. Nguyen, J. H. Shim, J. Electroanal. Chem., 2018, 827, 120-127.

8 Y. Lu, S. Zhao, R. Yang, D. Xu, J. Yang, Y. Lin, N.-E. Shi, Z. Dai, J. Bao, M. Han, ACS Appl. Mater. Interfaces, 2018, 10, 8155-8164.

9 S. Liu, H. Zhang, X. Mu, C. Chen, Appl. Catal., B, 2019, 241, 424-429.

10 H. Gong, X. Cao, F. Li, Y. Gong, L. Gu, R. G. Mendes, M. H. Rummeli, P. Strasser, R. Yang, ChemSusChem, 2017, 10, 1469-1474.

11 S. K. Konda, M. Amiri, A. Chen, J. Phys. Chem. C, 2016, 120, 14467-14473.

12 A. J. Jeevagan, T. Gunji, F. Ando, T. Tanabe, S. Kaneko, F. Matsumoto, J. Appl. Electrochem., 2016, 46, 745-753.